ADVANCED MATERIALS
www.advmat.de

Observation of Real-Time Spin-Orbit Torque Driven Dynamics in Antiferromagnetic Thin Film

Yang Cheng, Hanshen Huang, Junyu Tang, Joseph Lanier, Katelyn Lazareno, Hao-Kai Chang, Shang-Jui Chui, Chao-Yao Yang, Fengyuan Yang, Ran Cheng, and Kang L. Wang**

In the burgeoning field of spintronics, antiferromagnetic materials (AFMs) are attracting significant attention for their potential to enable ultra-fast, energy-efficient devices. Thin films of AFMs are particularly promising for practical applications due to their compatibility with spin-orbit torque (SOT) mechanisms. However, studying these thin films presents challenges, primarily due to the weak signals they produce and the rapid dynamics driven by SOT, that are too fast for conventional electric transport or microwave techniques to capture. The time-resolved magneto-optical Kerr effect (TR-MOKE) has been a successful tool for probing antiferromagnetic dynamics in bulk materials, thanks to its sub-picosecond (sub-ps) time resolution. Yet, its application to nanometer-scale thin films has been limited by the difficulty of detecting weak signals in such small volumes. In this study, the first successful observation of antiferromagnetic dynamics are presented in nanometer-thick orthoferrite films using the pump-probe technique to detect TR-MOKE signal. This paper report an exceptionally low damping constant of 1.5×10^{-4} and confirms the AFM magnonic nature of these dynamics through angular-dependent measurements. Furthermore, it is observed that electrical currents can potentially modulate these dynamics via SOT. The findings lay the groundwork for developing tunable, energy-efficient spintronic devices, paving the way for advancements in next-generation spintronic applications.

1. Introduction

Antiferromagnetic materials (AFM) are heralded as the future of spintronics, with their ultra-fast dynamics allowing for high-speed spin-orbit torque (SOT) switching—providing capabilities that could revolutionize spin-based technologies from high-density data storage for the next-generation computing architectures.[1–9] However, realizing the full potential of antiferromagnetic materials in spintronic applications has encountered substantial challenges. A majority of research only focused on electrical transport measurements by applying a current to these antiferromagnetic systems.[7,10–14] Despite the significant contributions of these studies, they have also sparked contentious debates regarding the actual switching speed and its mechanisms involved. The core issue is that traditional electrical transport and microwave measurement techniques cannot keep up with the ultra-fast timescales of antiferromagnetic dynamics, especially those induced by SOT. This technological gap makes it nearly

Y. Cheng, H. Huang, K. L. Wang
Department of Electrical and Computer Engineering, and Department of Physics and Astronomy
University of California
Los Angeles, CA 90095, USA
E-mail: cheng991@g.ucla.edu; wang@ee.ucla.edu

J. Tang, R. Cheng
Department of Physics and Astronomy
University of California
Riverside, CA 92507, USA

J. Lanier, K. Lazareno, F. Yang
Department of Physics
The Ohio State University
Columbus, OH 43210, USA

H.-K. Chang, C.-Y. Yang
Department of Materials Science and Engineering
National Yang Ming Chiao Tung University
Hsinchu 30010, Taiwan

S.-J. Chui
National Synchrotron Radiation Research Center
Taiwan 30074, Taiwan

R. Cheng
Department of Electrical and Computer Engineering
University of California
Riverside, CA 92521, USA

K. L. Wang
Department of Physics and Astronomy
University of California
Los Angeles, CA 90095, USA

The ORCID identification number(s) for the author(s) of this article can be found under https://doi.org/10.1002/adma.202417240

DOI: 10.1002/adma.202417240

impossible to acquire a detailed, time-resolved understanding as of how AFMs respond to current-induced SOT. Hence, there is an urgent need for new experimental approaches that can capture these exceedingly fast processes to unravel the nuanced behaviors and mechanisms at play.

A powerful alternative for probing antiferromagnetic dynamics is the time-resolved magneto-optical Kerr effect (TR-MOKE),[15–18] measured using the pump-probe technique. This highly sensitive approach has a proven track record in capturing fast magnetic dynamics. *While Terahertz (THz) emission spectroscopy provides valuable information by probing THz radiation,*[19–27] *TR-MOKE provides direct insights into the magnetization dynamics in magnetic materials*. For antiferromagnets, TR-MOKE has predominantly been used to study bulk systems, revealing phenomena such as inertia-driven spin switching and efficient magnetic field-induced spin precession in AFMs.[28–30] However, there is a critical gap in understanding antiferromagnetic dynamics in nanometer-thick films, which is essential for SOT applications because current must be applied at such scales to minimize energy and heat dissipation, as well as to counteract the decay of spin current.[7,11] The absence of investigations into thin film antiferromagnetic dynamics is primarily due to the challenge of weak signal emissions, a technical hurdle that hindered progress in this area.[15] Therefore, there's a compelling need to extend the capabilities of TR-MOKE or other time-domain techniques to nanoscale thin films to elucidate their dynamics and harness their potential for spintronics applications.

In this work, we make a significant leap forward by successfully probing the SOT-induced antiferromagnetic dynamics in a 30 nm thin film of $LaFeO_3$ (LFO) using the pump-probe technique. LFO is an orthoferrite and an example of the newly proposed class of magnetic materials called altermagnets[31] that are predicted to have strong magneto-optical effects. Notably, we observe an exceptionally low damping constant of 1.5×10^{-4}. Alongside this, we employ angular-dependent measurements to ensure that the observed signals and behaviors are ofa magnonic origin probed by quartic MOKE (QMOKE) signal. For the first time, we demonstrate the manipulation of antiferromagnetic dynamics using spin-orbit torque driven by electric current and capture these fast-paced dynamics in real-time.

2. Results

2.1. Characterization of the LFO Thin Films

LFO is an antiferromagnet with a relatively high Néel temperature (T_N) at 760 K.[32] Previously, researchers have utilized bulk LFO to explore antiferromagnetic dynamics, which informed our selection of this material. Our goal is to advance beyond previous studies by growing high-quality nanometer-thin LFO films to explore spin-orbit torque-driven antiferromagnetic dynamics. To achieve the required material quality in the study, we employed off-axis sputtering techniques to epitaxially grow the LFO film of 30 nm on $SrTiO_3$ (110) substrate (for a detailed description, see Methods). **Figure** 1a displays the X-ray diffraction pattern of the epitaxial heterostructure, which shows a remarkable crystalline quality as evidenced by the pronounced Laue oscillations. Conventionally, the Néel vector of a bulk LFO is along the **a**-axis of its orthorhombic lattice. However, for thin film LFO where **c**-axis is aligned to in-plane [001] orientation of $SrTiO_3$, crystallographic strain induced by the epitaxy would modify the uniaxial anisotropy of the LFO thin film to re-orientate the Néel order toward the **c**-axis[33] as depicted in Figure 1b. This modified AFM anisotropy induced the Néel order tilting was revealed by the X-ray magnetic linear dichroism (XMLD) spectroscopy. Figure 1c illustrates the experimental geometry of the XMLD, in which the X-ray absorption spectra (XAS) were acquired using a linearly polarized X-ray. The polarization, indicated by the electric field vector (E), was aligned at various incidence angles (θ) relative to the film normal. Note that, the sample rotation for the θ-dependent XAS was specifically configured within the **a-c** plane of the LFO film. This orientation was chosen to effectively resolve the tilting of the Néel order (see Methods for details). Figure 1d shows the θ-dependent XAS taken at the Fe L_2/L_3 edge, both featuring a double peak characteristic. As a result, while increasing the X-ray incidence angle, the intensity of low- (high)-energy state decreased (increased) at both L_2/L_3 edge and nearly got saturated at $\theta = 60°$, as highlighted in the inset of Figure 1d. The fine structure evolution on each L_2/L_3 edge suggests the Néel order of the investigated LFO film is deviating from the principal axes of the orthorhombic lattice, coinciding with the result in the previous study[33].

2.2. TR-MOKE Measurements in LFO Thin Films

To probe the ultrafast antiferromagnetic dynamics, we utilize the TR-MOKE in pump-probe scheme, as shown in **Figure** 2a (See Methods for more details). In our experimental setup, the initiation of antiferromagnetic dynamics is first achieved through thermal excitation by a linearly polarized pump pulse (400 nm, 1 mW) with normal incidence of light (See Section S4, Supporting Information)[16] This triggers a damped oscillation of the Néel vector along its equilibrium position. In the vanish of external field as well as spin orbit torque, the Néel vector processes with the antiferromagnetic resonance (AFMR) frequency along its local easy axis

$$f = \frac{\gamma}{2\pi}\sqrt{H_A\left(H_A + 2H_E\right)} \tag{1}$$

where γ is the gyromagnetic ratio, f is the AFMR frequency, H_E is the exchange field, H_A is the effective field of easy-axis anisotropy. To capture the ultrafast dynamics, we use the Kerr rotation effect on a subsequent linearly polarized probe pulse (800 nm, 15 μW) where we define φ as the angle between the polarization of probe pulse (P) and the in-plane projection of the Néel vector (n_{ip}). The key metric is the change in Kerr rotation as a function of the time delay between the pump and probe pulses (See Methods for details). This approach affords us a high temporal resolution, providing valuable insight into the rapid dynamical behaviors of antiferromagnetic materials compared to conventional methods. Ferromagnetic materials primarily exhibit first-order linear MOKE responses, where the signal is directly proportional to the out-of-plane component of the magnetization (m_z). In contrast, for antiferromagnets, the linear MOKE vanishes due to zero net magnetic moment. This leads to the detectability of a secondary effect known as quadratic MOKE (QMOKE), which can be effectively probed with its magnitude η proportional to

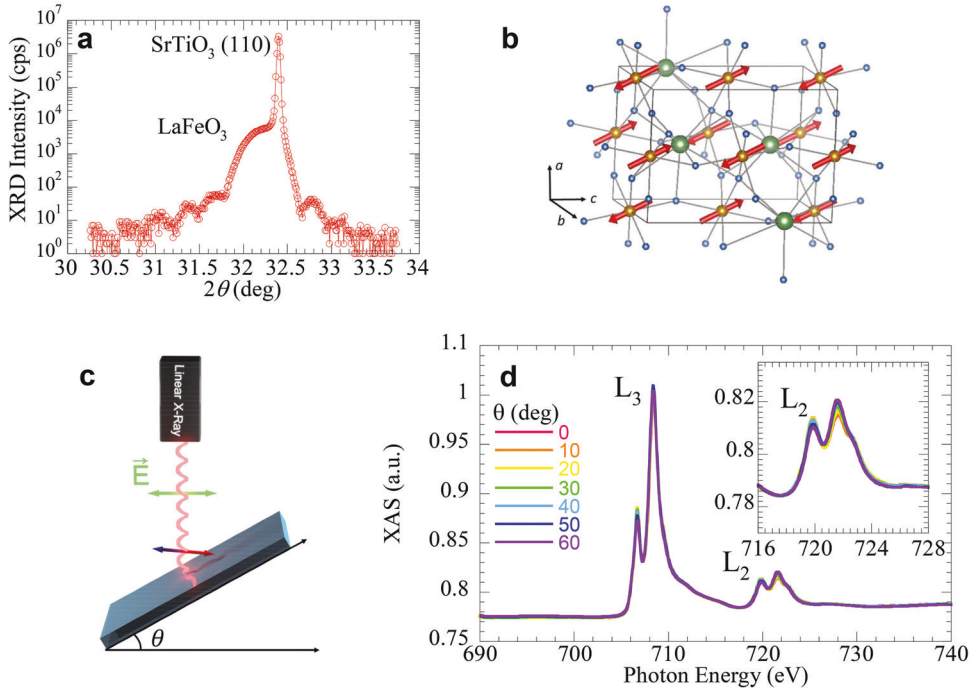

Figure 1. Crystal and spin structure of $LaFeO_3$. a) X-ray Diffractometry (XRD, $\lambda = 1.5405$ Å, Cu-K α) scan of the 30 nm thick $LaFeO_3$ layer grown on a $SrTiO_3$ (110) substrate, showcasing the crystal orientation of $LaFeO_3$. b) Spin structure of $LaFeO_3$ thin film grown on $SrTiO_3$ (110) substrate. Red arrows indicate the magnetic moments associated with Fe^{3+} ions. In bulk $LaFeO_3$, the easy axis aligns with the a-axis of the cell. However, a notable tilting of the Néel vector towards out of plane when $LaFeO_3$ is grown on the $SrTiO_3$ (110) substrate. c) Schematic of X-ray magnetic linear dichroism (XMLD). The x-rays incident on the sample at an angle θ relative to the sample surface, varies as the sample rotates about a vertical axis. d) X-ray Absorption Spectroscopy (XAS) of $LaFeO_3$ with varying θ. The angular dependence of the XAS spectrum at the L2 and L3 edges of Fe indicates that the easy axis is tilted toward the out-of-plane direction.

$\cos(2\varphi)$. Here, $\varphi = \varphi_{pr} - \varphi_n$ where φ_{pr} and φ_n are the in-plane projection direction of probe polarization (P) and Néel vector (n_{ip}), respectively. Therefore, the QMOKE signal is expected to exhibit an oscillation $\Delta\eta \propto \sin(2\varphi)\Delta n_{ip}(t)$.[14,34] Figure 2b shows TR-MOKE data with $\varphi = 45°$ where clear damped oscillations are observed. The pump-driven AFM dynamics are evaluated by fitting the TR-MOKE data $\Delta\eta$ with the phenomenological form[35]

$$\Delta\eta\ (t) = A_1\ \exp(-t/\tau)\sin\left(2\pi f t + \varphi_1\right) + A_2 \exp(-t/\nu) \quad (2)$$

where the first term shows the oscillation of the Néel vector with the amplitude of A_1, $\frac{1}{\tau} = \gamma\alpha(H_A + H_E)$, and α is the Gilbert damping constant (See Section S3 (Supporting Information) for more details of derivation). The second term is the background signal in the slow thermal relaxation process[36] From the fitting, $H_A = 80$ Oe and $f = 47.1$ Ghz are obtained, and we use $H_E = 1.8 \times 10^6$ Oe.[37,38] Notably, Gilbert damping constant $\alpha = 1.5 \times 10^{-4}$, which is comparable to the best magnetic insulators such as $Y_3Fe_5O_{12}$ (YIG)[39] (See Section S3 (Supporting Information) for the details of fitting). The excellent quality of our ultra-low damping LFO thin film allows us to observe such a weak MOKE signal using the reflection instead of the transmission setup, which is commonly used for bulk AFM system. Figure 2c illustrates angular dependent time-resolved measurements with varying φ. Figure 2d shows the extracted oscillation amplitude A_1 using Equation (2). The sin (2φ) dependency of A_1 confirms that the observed TR-MOKE signal observed is predominantly due to QMOKE.[14]

2.3. SOT Manipulation in LFO Thin Films

The major advantage of a thin film platform lies in its ability to facilitate the exploration of SOT induced dynamics. Following the observation of a strong QMOKE signal in the LFO thin film, we deposited a 5 nm layer of Pt on top of the LFO. Subsequently, we conducted pump-probe measurements while applying an DC electric current to induce SOT in the LFO layer. As illustrated in **Figure** 3a,b, TR-MOKE scans were performed with the current oriented parallel and perpendicular to the **y**-axis (**c**-axis) of the LFO, respectively. Notably, when the current was parallel to the **y**-axis, increasing the current density did not alter the TR-MOKE signal. This observation effectively rules out any thermal-induced drift in our device, especially considering that the maximum applied current density was a relatively modest 1.2×10^{10} A m^{-2}. On the other hand, with the current along to the x-axis, we detected a noticeable vertical shift in the TR-MOKE scan. This shift suggests that the antiferromagnetic (AFM) dynamics in the LFO thin film are being altered by the SOT induced by the applied current.

To gain insight into how SOT affects AFM dynamics, we developed an analytical model (See Section S3 Supporting Information for more details). This model, as depicted in **Figure** 4a,b,

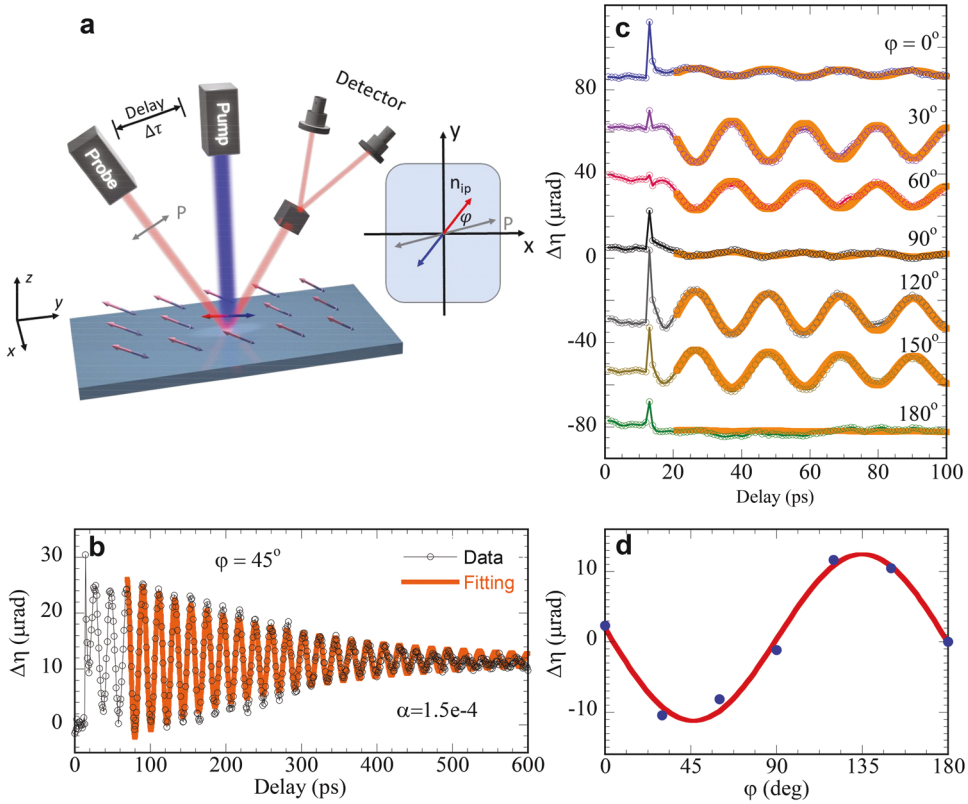

Figure 2. TR-MOKE measurement. a) Schematic of the TR-MOKE setup. The pump-probe measurement of the MOKE signal uses two linear-polarized lasers at 400 nm (pump) and 800 nm (probe), with the detection conducted via a balanced photodetector. Here, φ represents the relative angle between the in-plane projections of the probe polarization and the Néel vector. b) Oscillations of the MOKE signal for the polarization rotation measured at $\varphi = 45°$. The damping constant can be extracted by fitting the damped oscillations curves. c) Evolution of the MOKE signal with varied φ. d) Angular dependence of MOKE magnitude A_1 extracted by Equation (1). The sin2φ dependence as shown in the red curve confirms that the quadratic MOKE is the dominant contributor to the MOKE signal, serving as a probe for the in-plane projections of the Néel vector.

elucidates the shift in the equilibrium position triggered by a field-like (FL) and a damping-like (DL) SOT when the currents flow parallel and perpendicular to the y-axis, respectively. These shifts result from the solution of torque-balance equations. Intriguingly, FL-SOT exerts a minimal effect on the AFM spin, regardless of current direction. However, DL-SOT has a more pronounced influence. Specifically, when the current aligns with the y-axis, DL-SOT induces rotation of the Néel vector within the yz-plane by an angle $\Delta\theta$, without altering the in-plane (xy-plane) projection of the Néel vector. However, when the current runs perpendicular to the y-axis, DL-SOT causes the Néel vector to rotate in the xy′-plane by an angle $\Delta\varphi'$, where the y′-axis is the Néel vector's direction. This rotation prompts a corresponding shift in the in-plane projection of the Néel vector by $\Delta\varphi = \Delta\varphi'/\cos\theta_0$, where $\theta_0 = \sphericalangle(\mathbf{y}, \boldsymbol{n}_0)$ signifies the tilted angle between y and Néel vector $\boldsymbol{n}_0$. Now we move to investigate how DL-SOT affects time-resolved scans. Figure 4c,d display simulations of the oscillating $\Delta\varphi_n$, which correspond to the QMOKE signal. The ultrafast demagnetization performs as displacing the Néel vector from its equilibrium and then employing the Landau-Lifshitz-Gilbert (LLG) equation, augmented with the SOT term, for dynamic simulation. As a result, currents along the y-axis do not alter the oscillation pattern, while currents perpendicular to the x-axis introduce a vertical shift, both consistent with the experimental observations. The different behaviors observed in TR-MOKE in response to varying current directions stem from the fact that QMOKE is more sensitive to changes of the in-plane projection of the Néel vector. Thus, DL-SOT applied perpendicularly to the y-axis results in more significant alterations. Moreover, our model effectively demonstrates that the DL-SOT is the predominant factor influencing AFM dynamics, in contrast to the negligible role of FL-SOT, in time domain. Additionally, the influence of SOT on the AFMR frequency is minor, as the effective SOT field is too small compared to the anisotropy fields. However, we acknowledge that the model predicts a change in oscillation amplitude with varying current densities as shown in Figure 4(d), which was not observed experimentally. This discrepancy may result from limitations in experimental precision due to the inherently weak signal in the nanometer-thin film. Despite this, the vertical shift unique to DL-SOT strongly supports its role in driving the observed dynamics.

3. Discussion

The development and control of antiferromagnetic materials at the nanoscale represents one of the most promising yet challenging frontiers in spintronics. Our work serves as a pioneering study in this evolving domain, unlocking new possibilities for

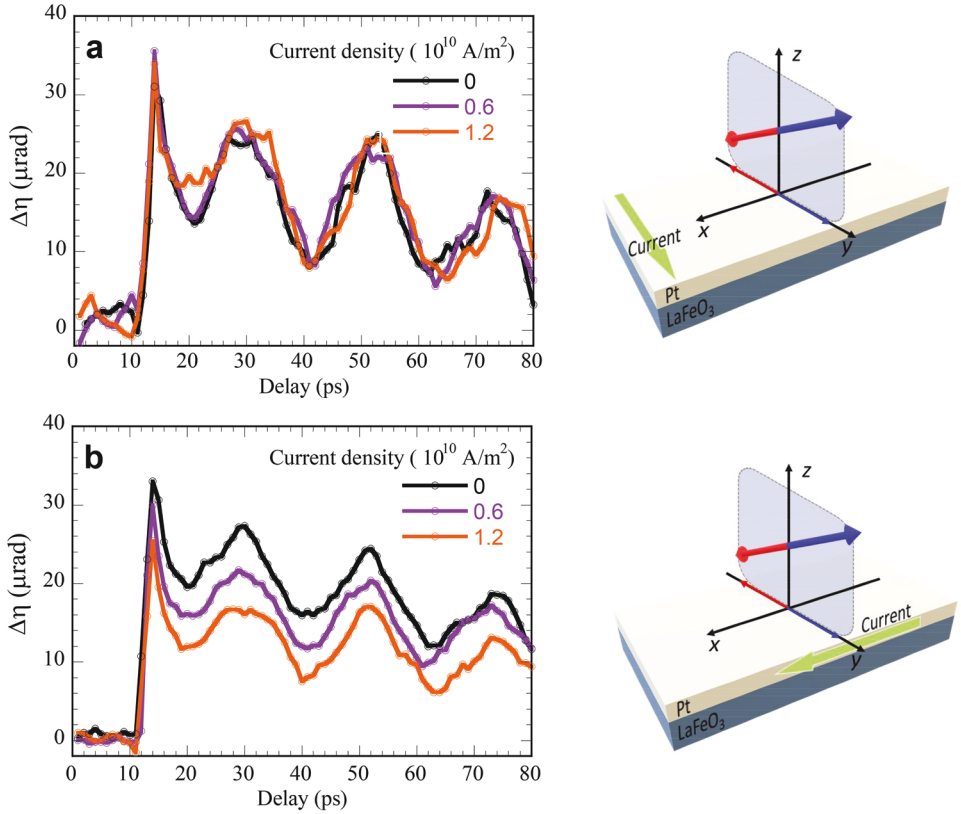

Figure 3. Current induced dynamics for the $LaFeO_3$/Pt bilayers. a) When the current is applied along $\hat{y}$-axis, there is no change of QMOKE signal. b) When the current is applied along $\hat{x}$-axis, a vertical shift is observed.

ultrafast and energy-efficient applications. We have demonstrated for the first time the ability to observe and manipulate ultrafast antiferromagnetic dynamics using TR-MOKE in nanometer-thick thin films. Overcoming the limitations posed by weak signals in nanometer-thin films helps us reveal important insights into antiferromagnetic dynamics. Our measurements show a remarkably low damping constant of our LFO thin film, and more importantly, suggest that SOT can influence these rapid antiferromagnetic dynamics. Our successful use of SOT to control these dynamics paves the way for the development of next-generation spintronic devices that promise unparalleled speed and energy efficiency. The application of TR-MOKE allows us to go beyond the constraints of conventional electrical transport measurements, offering a more nuanced and high-resolution view of antiferromagnetic behaviors. This capability is particularly invaluable for capturing phenomena that are too fast for traditional methods, serving as a new diagnostic tool for researchers in the field, thereby opening new avenues in ultrafast spintronics.

4. Experimental Section

Sample Preparation: High quality epitaxial $LaFeO_3$ films were grown on $SrTiO_3$ substrate with an off-axis sputtering system with a base pressure lower than 1×10^{-8} Torr at 650 °C. Substrates were undergone solvent (Acetone and IPA) cleaning with light sonication. As shown in Figure S1 (Supporting Information), atomic force microscopy shows both films being atomically smooth with roughness below 0.3 nm. The magnetic hysteresis loops of a $LaFeO_3$ (30 nm) only shows a very small magnetization due to canting of the Néel vector by the Dzyaloshinskii–Moriya Interaction (DMI).

TR-MOKE Setup: Femtosecond pulses (FWHM = 200 fs, 800 nm; pulse energy, 1 μJ) were generated by Spitfire (Spectra Physics) with a repetition rate of 1KHz. The pulse was then separated into the pump pulse and the probe pulse by a beam splitter. The pump pulse goes through a Beta Barium Borate (BBO) crystal and was converted from the 800 nm light to 400 nm and shine on the sample surface obliquely to excite the LFO with fluence, 6 mJ cm^{-2}. A mechanical chopper (37Hz) was applied to the pump arm to increase the signal quality. The probe light goes through a delay line and shines on the sample surface normally. The reflected light was separated into the P and S waves by a Wollaston Prism and collected by a Balanced Photodiode. The collected signal was then demodulated by a Lock-in Amplifier (Stanford Research 380). By changing the time delay between the arrival times of the pump pulse and probe pulse, the spin dynamic information was thus extracted.

It should be noted that the 45° measurement in Figure 2(b) and the angular dependence measurements in Figure 2(c) were performed separately. The angular dependence measurements in Figure 2(c) were conducted continuously from 0° to 180° in 30° intervals, while the 45° measurement in Figure 2(b) was an independent measurement which involved recalibrating the optical path that can cause slight shifts in the extracted amplitude A_1. Thus, Figure 2(d) only summarizes the fitting of A_1 extracted from Figure 2(c) to ensure consistency. However, the intrinsic parameters, such as f and $\frac{1}{\tau}$ remain unaffected across measurements and were confirmed by the fitting in both (Figure 2b,c).

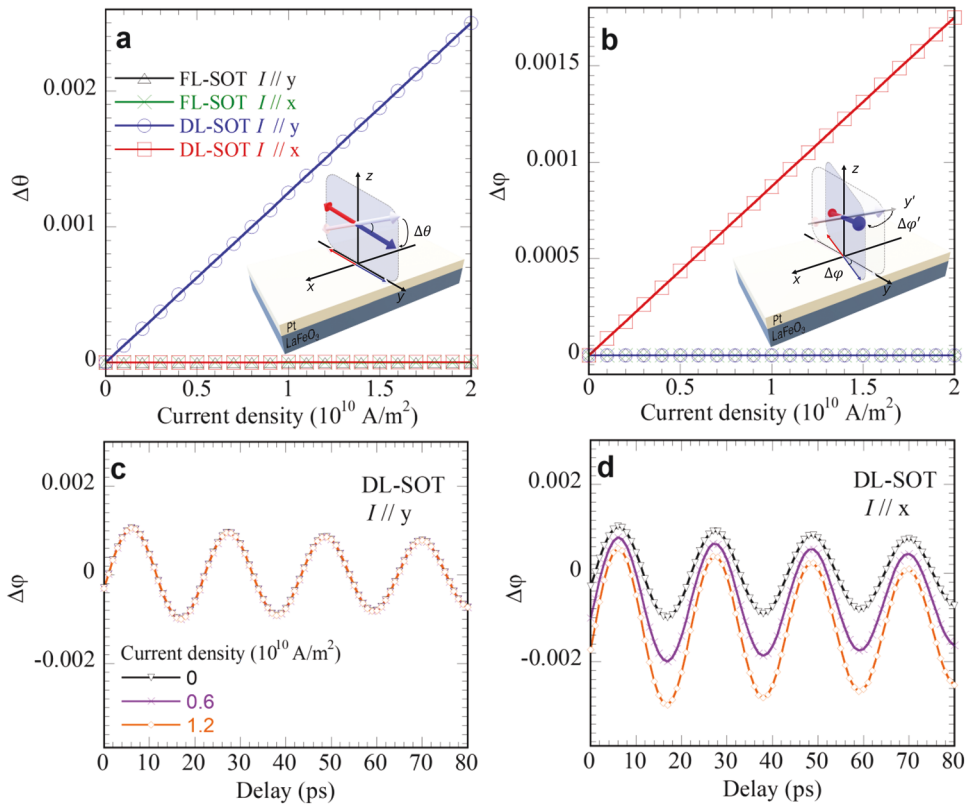

Figure 4. SOT induced AFM dynamics. a and b) Field-like (FL-) and damping-like (DL-) SOT induced rotation of Néel vector for current I // $\hat{y}$-axis and // $\hat{x}$-axis. Inset illustrates the rotations in different planes. The FL-SOT results in negligible changes of Néel vector. In contrast, with DL-SOT, a considerable rotation of $\Delta\theta$ is observed in the yz-plane when I // $\hat{y}$-axis. Similarly, when current aligns with $\hat{x}$ -axis, the Néel vector undergoes a rotation in the y′x-plane, leading to an in-plane (xy-plane) rotation of $\Delta\varphi'$. c) Simulated TR-MOKE oscillation with DL-SOT generated for I // $\hat{y}$-axis. No significant change is observed for different current densities in this configuration. d) Simulated TR-MOKE oscillation when DL-SOT generated by I // $\hat{x}$ -axis where there is a notable vertical shift of the curves is observed. It is attributed to the QMOKE is more sensitive to the in-plane rotation of the Néel vector induced by SOT.

XMLD Setup: The X-ray absorption spectrum (XAS) measurements were performed at the beamline 11A of National Synchrotron Radiation Research Center (NSRRC), Taiwan. The X-ray incidence was linearly polarized and shined on the LFO sample with an incidence angle (θ) to the film normal direction, where the $\theta = 0°$ was defined as the normal incidence illustrated in Figure 1c. All the XAS taken with various θ were all analyzed by aligning the pre-edge intensity to be zero and then normalized the spectra by the post-edge intensity to make all the XAS superimposed for the fine structure comparison. The sample was kept at 300 K during the measurement and the chamber pressure was kept around 5×10^{-9} torr.

Supporting Information

Supporting Information is available from the Wiley Online Library or from the author.

Acknowledgements

Y.C., and H.H. contributed equally to this work. K.L.W supervised the work. The authors at the University of California, Los Angeles acknowledge the support from the National Science Foundation (NSF) Award No. 1411085, No. 1810163, and No. 1611570; and the Army Research Office Multidisciplinary University Research Initiative (MURI) under grant numbers W911NF16-1-0472 and W911NF-19-S-0008. The work at University of California, Riverside was supported by the Air Force Office of Scientific Research under Grant No. FA9550-19-1-0307. F.Y., and D.R. at The Ohio State University acknowledges support from the Center for Emergent Materials, an NSF MRSEC, under Grant No. DMR-2011876, and NSF award No. DMR-2225646. H.K.C. and C.Y.Y. acknowledge the support of National Science and Technology Council (NSTC) under Grant No. 112-2112-M-A49-026 and acknowledge the technical support of X-ray spectroscopy from Mr. F.-H.C. and Dr. H.-J.L. at National Synchrotron Radiation Research Center (NSRRC), Taiwan.

Conflict of Interest

The authors declare no conflict of interest.

Author Contributions

Y.C. designed, planned and initiated the study. H.H. performed TR-MOKE measurement. J.Y.T., and R.C. contributed to the theoretical modeling of QMOKE. J.L., K.L, and F.Y.Y. grew the LFO films. H. K. C. performed the XMLD measurement and analyzed the XMLD data with C.Y.Y. K.L.W. supervised the project. Y.C., H.H., J.Y.T., J.L., C.Y.Y., and K.L.W. drafted the manuscript. All authors discussed the results and commented on the manuscript.

Data Availability Statement

The data that support the findings of this study are available from the corresponding author upon reasonable request.

Keywords

antiferromagnetic, spin-orbit torque, spintronics, TR-MOKE

Received: November 8, 2024
Revised: December 27, 2024
Published online: January 26, 2025

[1] T. Jungwirth, X. Marti, P. Wadley, J. Wunderlich, *Nat. Nanotechnol.* **2016**, *11*, 231.
[2] V. Baltz, A. Manchon, M. Tsoi, T. Moriyama, T. Ono, Y. Tserkovnyak, *Rev. Mod. Phys.* **2018**, *90*, 015005.
[3] T. Kampfrath, A. Sell, G. Klatt, A. Pashkin, S. Mährlein, T. Dekorsy, M. Wolf, M. Fiebig, A. Leitenstorfer, R. Huber, *Nat. Photonics* **2011**, *5*, 31.
[4] X. Marti, I. Fina, C. Frontera, J. Liu, P. Wadley, Q. He, R. J. Paull, J. D. Clarkson, J. Kudrnovský, I. Turek, J. Kunes, D. Yi, J.-H. Chu, C. T. Nelson, L. You, E. Arenholz, S. Salahuddin, J. Fontcuberta, T. Jungwirth, R. Ramesh, *Nat. Mater.* **2014**, *13*, 367.
[5] J. Shi, V. Lopez-Dominguez, F. Garesci, C. Wang, H. Almasi, M. Grayson, G. Finocchio, P. Khalili Amiri, *Nat. Electron.* **2020**, *3*, 92.
[6] O. Gomonay, T. Jungwirth, J. Sinova, *Phys. Rev. Lett.* **2016**, *117*, 017202.
[7] Y. Cheng, S. Yu, M. Zhu, J. Hwang, F. Yang, *Phys. Rev. Lett.* **2020**, *124*, 027202.
[8] Y. Deng, X. Liu, Y. Chen, Z. Du, N. Jiang, C. Shen, E. Zhang, H. Zheng, H.-Z. Lu, K. Wang, *Natl. Sci. Rev.* **2023**, *10*, nwac154.
[9] X. Liu, Q. Feng, D. Zhang, Y. Deng, S. Dong, E. Zhang, W. Li, Q. Lu, K. Chang, K. Wang, *Adv. Mater.* **2023**, *35*, 2211634.
[10] P. Zhang, J. Finley, T. Safi, L. Liu, *Phys. Rev. Lett.* **2019**, *123*, 247206.
[11] P. Wadley, B. Howells, J. Zelezný, C. Andrews, V. Hills, R. P. Campion, V. Novák, K. Olejník, F. Maccherozzi, S. S. Dhesi, S. Y. Martin, T. Wagner, J. Wunderlich, F. Freimuth, Y. Mokrousov, J. Kunes, J. S. Chauhan, M. J. Grzybowski, A. W. Rushforth, K. W. Edmonds, B. L. Gallagher, T. Jungwirth, *Science* **2016**, *351*, 587.
[12] S. Y. Bodnar, L. Smejkal, I. Turek, T. Jungwirth, O. Gomonay, J. Sinova, A. A. Sapozhnik, H.-J. Elmers, M. Kläui, M. Jourdan, *Nat. Commun.* **2018**, *9*, 34.
[13] X. Z. Chen, R. Zarzuela, J. Zhang, C. Song, X. F. Zhou, G. Y. Shi, F. Li, H. A. Zhou, W. J. Jiang, F. Pan, Y. Tserkovnyak, *Phys. Rev. Lett.* **2018**, *120*, 207204.
[14] Y. Cheng, E. Cogulu, R. D. Resnick, J. J. Michel, N. N. Statuto, A. D. Kent, F. Yang, *Nat. Commun.* **2022**, *13*, 3659.
[15] P. Němec, M. Fiebig, T. Kampfrath, A. V. Kimel, *Nat. Phys.* **2018**, *14*, 229.
[16] V. Saidl, P. Nemec, P. Wadley, V. Hills, R. P. Campion, V. Novák, K. W. Edmonds, F. Maccherozzi, S. S. Dhesi, B. L. Gallagher, F. Trojánek, J. Kunes, J. Zelezný, P. Malý, T. Jungwirth, *Nat. Photonics* **2017**, *11*, 91.
[17] A. Kimel, A. Kirilyuk, A. Tsvetkov, R. Pisarev, T. Rasing, *Nature* **2004**, *429*, 850.
[18] J. R. Hortensius, D. Afanasiev, M. Matthiesen, R. Leenders, R. Citro, A. V. Kimel, R. V. Mikhaylovskiy, B. A. Ivanov, A. D. Caviglia, *Nat. Phys.* **2021**, *17*, 1001.
[19] H. Qiu, L. Zhou, C. Zhang, J. Wu, Y. Tian, S. Cheng, S. Mi, H. Zhao, Q.i Zhang, D.i Wu, B. Jin, J. Chen, P. Wu, *Nat. Phys.* **2021**, *17*, 388.
[20] E. Rongione, O. Gueckstock, M. Mattern, O. Gomonay, H. Meer, C. Schmitt, R. Ramos, T. Kikkawa, M. Micica, E. Saitoh, J. Sinova, H. Jaffrès, J. Mangeney, S. T. B. Goennenwein, S. Geprägs, T. Kampfrath, M. Kläui, M. Bargheer, T. S. Seifert, S. Dhillon, R. Lebrun, *Nat. Commun.* **2023**, *14*, 1818.
[21] Y. Behovits, A. L. Chekhov, S. Y.u. Bodnar, O. Gueckstock, S. Reimers, Y. Lytvynenko, Y. Skourski, M. Wolf, T. S. Seifert, O. Gomonay, M. Kläui, M. Jourdan, T. Kampfrath, *Nat. Commun.* **2023**, *14*, 6038.
[22] S. Schlauderer, C. Lange, S. Baierl, T. Ebnet, C. P. Schmid, D. C. Valovcin, A. K. Zvezdin, A. V. Kimel, R. V. Mikhaylovskiy, R. Huber, *Nature* **2019**, *569*, 383.
[23] R. V. Mikhaylovskiy, E. Hendry, V. V. Kruglyak, R. V. Pisarev, T.h. Rasing, A. V. Kimel, *Phys. Rev. B* **2014**, *90*, 184405.
[24] R. V. Mikhaylovskiy, E. Hendry, A. Secchi, J. H. Mentink, M. Eckstein, A. Wu, R. V. Pisarev, V. V. Kruglyak, M. I. Katsnelson, T.h. Rasing, A. V. Kimel, *Nat. Commun.* **2015**, *6*, 8190.
[25] R. V. Mikhaylovskiy, T. J. Huisman, A. I. Popov, A. K. Zvezdin, T. H. Rasing, R. V. Pisarev, A. V. Kimel, *Phys. Rev. B* **2015**, *92*, 094437.
[26] R. Mikhaylovskiy, T. Huisman, R. Pisarev, T. Rasing, A. Kimel, *Physical Rev. Lett.* **2017**, *118*, 017205.
[27] R. V. Mikhaylovskiy, T. J. Huisman, V. A. Gavrichkov, S. I. Polukeev, S. G. Ovchinnikov, D. Afanasiev, R. V. Pisarev, T. Rasing, A. V. Kimel, *Phys. Rev. Lett.* **2020**, *125*, 157201.
[28] T. F. Nova, A. Cartella, A. Cantaluppi, M. Först, D. Bossini, R. V. Mikhaylovskiy, A. V. Kimel, R. Merlin, A. Cavalleri, *Nat. Phys.* **2017**, *13*, 132.
[29] A. V. Kimel, B. A. Ivanov, R. V. Pisarev, P. A. Usachev, A. Kirilyuk, T. Rasing, *Nat. Phys.* **2009**, *5*, 727.
[30] D. Yang, T. Kim, K. Lee, C. Xu, Y. Liu, F. Wang, S. Zhao, D. Kumar, H. Yang, *Nat. Commun.* **2024**, *15*, 4046.
[31] R. A. Leenders, D. Afanasiev, A. V. Kimel, R. Mikhaylovskiy, *Nature* **2024**, *630*, 335.
[32] W. Lin, J. He, B. Ma, M. Matzelle, J. Xu, J. Freeland, Y. Choi, D. Haskel, B. Barbiellini, A. Bansil, G. A. Fiete, J. Zhou, C. L. Chien, *Nat. Phys.* **2022**, *18*, 800.
[33] J. Lüning, F. Nolting, A. Scholl, H. Ohldag, J. W. Seo, J. Fompeyrine, J.-P. Locquet, J. Stöhr, *Phys. Rev. B* **2003**, *67*, 214433.
[34] C. Tzschaschel, K. Otani, R. Iida, T. Shimura, H. Ueda, S. Günther, M. Fiebig, T. Satoh, *Phys. Rev. B* **2017**, *95*, 174407.
[35] S. Mizukami, F. Wu, A. Sakuma, J. Walowski, D. Watanabe, T. Kubota, X. Zhang, H. Naganuma, M. Oogane, Y. Ando, T. Miyazaki, *Phys. Rev. Lett.* **2011**, *106*, 117201.
[36] D.-L. Zhang, J. Zhu, T. Qu, D. M. Lattery, R. H. Victora, X. Wang, J.-P. Wang, *Sci. Adv.* **2020**, *6*, eabb4607.
[37] I. Ameri, A. Boularaf, F. Drief, A. Zaoui, S. Kacimi, *J. Magn. Magn. Mater.* **2021**, *537*, 168214.
[38] K. Park, H. Sim, J. C. Leiner, Y. Yoshida, J. Jeong, S.-i. Yano, J. Gardner, P. Bourges, M. Klicpera, V. Sechovský, M. Boehm, J.-G. Park, *J. Phys.: Condens. Matter* **2018**, *30*, 235802.
[39] H. L. Wang, C. H. Du, Y. Pu, R. Adur, P. C. Hammel, F. Y. Yang, *Phys. Rev. Lett.* **2014**, *112*, 197201.